Inorganic Chemistry

Article

pubs.acs.org/IC

# Differentially Selective Chemosensor with Fluorescence *Off–On* Responses on $Cu^{2+}$ and $Zn^{2+}$ Ions in Aqueous Media and Applications in Pyrophosphate Sensing, Live Cell Imaging, and Cytotoxicity

Sellamuthu Anbu,[†] Rajendran Ravishankaran,[‡] M. Fátima C. Guedes da Silva,[†] Anjali A. Karande,[‡] and Armando J. L. Pombeiro*[,†]

[†]Centro de Química Estrutural, Complexo I, Instituto Superior Técnico, Universidade de Lisboa, Avenida Rovisco Pais, 1049-001 Lisboa. Portugal

[‡]Department of Biochemistry, Indian Institute of Science, Bangalore 560 012, India

Supporting Information

**ABSTRACT:** A new benzoyl hydrazone based chemosensor **R** is synthesized by Schiff base condensation of 2,6-diformyl-4-methylphenol and phenyl carbohydrazide and acts as a highly selective fluorescence sensor for $Cu^{2+}$ and $Zn^{2+}$ ions in aqueous media. The reaction of **R** with $CuCl_2$ or $ZnCl_2$ forms the corresponding dimeric dicopper(II) $[Cu_2(R)(CH_3O)(NO_3)]_2(CH_3O)_2$ (**R-Cu$^{2+}$**) and dizinc(II) $[Zn_2(R)_2](NO_3)_2$ (**R-Zn$^{2+}$**) complexes, which are characterized, as **R**, by conventional techniques including single-crystal X-ray analysis. Electronic absorption and fluorescence titration studies of **R** with different metal cations in a $CH_3CN$/0.02 M HEPES buffer medium (pH = 7.3) show a highly selective binding affinity only toward $Cu^{2+}$and $Zn^{2+}$ ions even in the presence of other commonly coexisting ions such as $Na^+$, $K^+$, $Mg^{2+}$, $Ca^{2+}$, $Mn^{2+}$, $Fe^{2+}$, $Fe^{3+}$, $Co^{2+}$, $Ni^{2+}$, $Cd^{2+}$, and $Hg^{2+}$. Quantification of the fluorescence titration analysis shows that the chemosensor **R** can indicate the presence of $Cu^{2+}$and $Zn^{2+}$ even at very low concentrations of 17.3 and 16.5 ppb, respectively. **R-Zn$^{2+}$** acts as a selective metal-based fluorescent sensor for inorganic pyrophosphate ion (PPi) even in the presence of other common anions such as $F^-$, $Cl^-$, $Br^-$, $I^-$, $CH_3COO^-$, $CO_3^{2-}$, $HCO_3^-$, $N_3^-$, $SO_4^{2-}$, PPi, AMP, ADP, and ATP in an aqueous medium. The propensity of **R** as a bioimaging fluorescent probe to detect $Cu^{2+}$ and $Zn^{2+}$ ions in human cervical HeLa cancer cell lines and their cytotoxicity against human cervical (HeLa), breast cancer (MCF7), and noncancer breast epithelial (MCF10a) cells have also been investigated. **R-Cu$^{2+}$** shows better cytotoxicity and sensitivity toward cancer cells over noncancer cells than **R** and **R-Zn$^{2+}$** under identical conditions, with the appearance of apoptotic bodies.

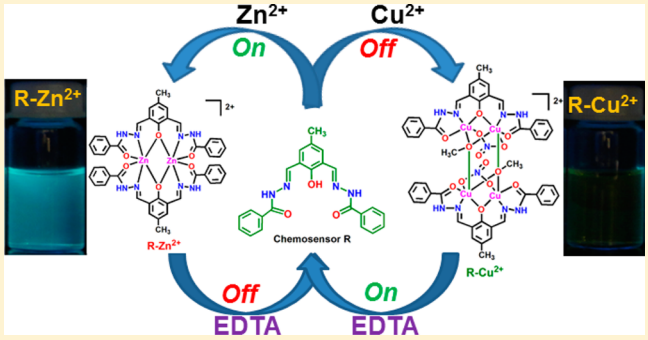


## INTRODUCTION

Investigation on molecular fluorescent chemosensing of metal ions is a promising research field in chemistry with established roles in ecological, biological, and clinical applications.[1] In particular, fluorescent chemosensors have several advantages over other optical sensors because of their intrinsic high sensitivity, ease of handling, and real-time monitoring with fast response time.[2] In light of this dispute, sensing copper and zinc ions in aqueous media is biochemically relevant because of their crucial roles in biological systems.[3] $Cu^{2+}$ ion is a vital (both useful and cytotoxic) trace ion in various enzymatic processes, is required as a cofactor for many fundamental biological processes, and catalyzes the production of highly reactive oxygen species,[4] connected to serious neurodegenerative illnesses such as Alzheimer's, Wilson's, and Menke's diseases.[5] Similarly, a wide repertoire of $Zn^{2+}$-based compounds have been utilized as radioprotective agents,[6] tumor photosensitizers,[7] antidiabetic insulin mimetic,[8] and antibacterial or antimicrobial and anticancer agents.[9] $Zn^{2+}$ can also reduce the cardio- and hepatotoxicity induced by some anticancer drugs.[10] In recent times, a number of selective and sensitive imaging tools capable of rapidly monitoring $Cu^{2+}$ and $Zn^{2+}$ ions have developed.[11] However, single chemosensors that discriminate metal ions selectively from others in an *off–on* manner are sparse.[12] Hence, the sensing of two metal ions by a single chemosensor in an aqueous medium and the use of a single technique displaying distinct outputs for different ions are essential. In the context of the above objectives, in this work, we have synthesized a highly sensitive (nanomolar) and selective benzoyl hydrazone based new visual and fluorescent chemosensor **R** for $Cu^{2+}$ and $Zn^{2+}$ ions, screened its potential applications in human cancer cell imaging and pyrophosphate sensing, and studied its cytotoxic properties.

**Received:** February 8, 2014
**Published:** June 12, 2014

   dx.doi.org/10.1021/ic500313m | *Inorg. Chem.* 2014, 53, 6655–6664

## EXPERIMENTAL SECTION

**Materials and Measurements.** All of the materials for the synthesis of **R** were purchased from various commercial sources and used without further purification. A spectroscopic-grade $CH_3CN$ solvent was used for all titration experiments. $^1H$ and $^{13}C$ NMR spectra were run on a Bruker 400 MHz spectrometer. The chemical shifts ($\delta$) are reported in parts per million (ppm) relative to tetramethylsilane ($Me_4Si$) as the internal standard (0.0 ppm) or (for $^1H$ NMR spectra) proton resonance resulting from incomplete deuteration of the NMR solvent: dimethyl sulfoxide (DMSO)-$d_6$. IR spectra were recorded on a Bruker Alpha Fourier transform infrared (FTIR) spectrometer. Electronic absorption spectral measurements were done using a PerkinElmer Lambda 750 UV−visible spectrophotometer, and the fluorescence emission studies were carried out on a Horiba Jobin-Yvon Fluoromax-4 spectrometer. Electrospray ionization mass spectrometry (ESI-MS) spectra of the compounds were recorded on a Varian 500 mass spectrometer.

*Synthesis of the Chemosensor* ***R.*** A methanolic solution (15 mL) of of 2,6-diformyl-4-methylphenol (0.5 g, 3 mmol) was added slowly to phenyl carbohydrazide (0.83 g, 6 mmol) in methanol, and the mixture was stirred for 4 h at 50 °C. A yellow precipitate was collected by filtration and washed several times with cold methanol. The obtained yellow crystalline material was recrystallized from an acetonitrile solution. Isolated yield: yellow crystals, 0.82 g (62%). Anal. Calcd for $C_{23}H_{20}N_4O_3$: C, 68.99; H, 5.03; N, 13.99. Found: C, 69.07; H, 5.09; N, 13.93. IR (KBr, $cm^{-1}$): $\nu$ 3272s (−NH), 3212br (−OH), 3055s (−NH), 1668s (−C═O), 1636s (−C═N), 997s (−N−N). $^1H$ NMR (DMSO-$d^6$, 400 MHz): $\delta$ 12.33 (s, H, phenolic OH), 11.60 (s, 2H, NH), 8.73 (s, 2H, CH═N), 7.95 (dd, 4H, $J$ = 8.8 Hz, H−phenyl), 7.61 (dd, 4H, $J$ = 8.6 Hz, H−phenyl), 7.58 (d, 2H, $J$ = 8.6 Hz, H−phenyl), 7.55 (s, 2H, H− phenyl), 2.45 (s, 3H, H−methyl). $^{13}C$ NMR (DMSO-$d^6$, 100 MHz): $\delta$ 20.38, 120.39, 128.14, 128.70, 129.00, 130.83, 132.43, 133.37, 146.58, 155.17, 163.40. ESI-MS in $CH_3OH$. Calcd for $[\mathbf{R} + Na^+]^+$: $m/z$ 423.14. Found: $m/z$ 423.31.

*Synthesis of the Dimeric Dicopper(II) Complex* ***[Cu$_2$(R)(CH$_3$O)(NO$_3$)]$_2$(CH$_3$O)$_2$ (R-Cu$^{2+}$).*** An ethanolic solution (10 mL) of copper(II) chloride dihydrate (0.26 g, 1.5 mmol) was added slowly to the receptor **R** (0.3 g, 0.75 mmol) in ethanol with continuous stirring. The solution turned pale green. Sodium nitrate (0.15 g, 1.7 mmol) was added to the resulting pale-green solution and the system refluxed for 2 h. A pale-green solid precipitate was collected by filtration, washed several times with cold ethanol, and dried in vacuum. Pale-green crystals suitable for X-ray analysis were obtained after 2 weeks by the slow evaporation of a methanol solution. Yield: pale-green crystals, 0.38 g (68%). IR (KBr, $cm^{-1}$): $\nu$ 3465s (N−H), 1689s (C═O), 1639s (C═N), 1443vs (N−O), 1246s (N−O), 1012s (−N−N). $\lambda_{max}$, nm ($\varepsilon$, $M^{-1}$ $cm^{-1}$) in $CH_3CN$: 643 (370), 423 (22500), 346 (29700), 302 (48500). Anal. Calcd for $C_{50}H_{50}Cu_4N_{10}O_{16}$: C, 46.15; H, 3.87; N, 10.76; Cu, 19.67. Found: C, 46.27; H, 3.79; N, 10.85; Cu, 19.40. ESI-MS in $CH_3OH$: $m/z$ 1079.62 ($[Cu_4(R)_2(OCH_3) - 2NO_3 - 3OCH_3 + H^+]^+$), 557.15 ($[Cu_2(R)(OCH_3)_2 - OCH_3 - NO_3 + H^+]^+$).

*Synthesis of the Dizinc(II) Complex* ***[Zn$_2$(R)$_2$](NO$_3$)$_2$ (R-Zn$^{2+}$).*** The dinuclear complex **R-Zn$^{2+}$** has been synthesized by following the above procedure using zinc(II) chloride (0.20 g, 1.5 mmol) instead of copper(II) chloride dihydrate. Yield: pale-yellow crystals, 0.39 g (78%). IR (KBr, $cm^{-1}$): $\nu$ 3467s (N−H), 1683s (C═O), 1634s (C═N), 1359vs (N−O), 1008s (−N−N), 822s (N−O). $^1H$ NMR (DMSO-$d^6$, 400 MHz): $\delta$ 11.58 (s, 4H, NH), 8.74 (s, 4H, CH═N), 7.96 (dd, 8H, $J$ = 8.8 Hz, H−phenyl), 7.62 (dd, 8H, $J$ = 8.6 Hz, H−phenyl), 7.58 (d, 4H, $J$ = 8.6 Hz, H−phenyl), 7.55 (s, 4H, H−phenyl), 2.43 (s, 6H, H−methyl). $\lambda_{max}$, nm ($\varepsilon$, $M^{-1}$ $cm^{-1}$) in $CH_3CN$: 415 (18500), 305 (32500). Anal. Calcd for $C_{46}H_{38}N_{10}O_{12}Zn_2$: C, 52.54; H, 3.64; N, 13.29; Zn, 12.41. Found: C, 52.64; H, 3.69; N, 13.35; Zn, 12.50. ESI-MS in $CH_3OH$: $m/z$ 929.44 ($[Zn_2(R)_2 - 2NO_3 + H^+]^+$), 465.35 ($[Zn_2(R)_2 - 2NO_3]^{2+}$).

**X-ray Crystallography.** X-ray-quality single crystals of the compounds were immersed in cryo-oil, mounted in a nylon loop, and measured at 150 K (**R-Cu$^{2+}$**) or at room temperature (**R-Zn$^{2+}$**). Intensity data were collected using a Bruker AXS-Kappa APEX II or a Bruker APEX-II PHOTON 100 diffractometer with graphite-monochromated Mo K$\alpha$ ($\lambda$ = 0.71069 nm) radiation. Data were collected using $\phi$ and $\omega$ scans of 0.5° frame$^{-1}$, and a full sphere of data was obtained. Cell parameters were retrieved using Bruker *SMART* software[1] and refined using Bruker *SAINT*[13a] on all of the observed reflections. Absorption corrections were applied using *SADABS*.[13a] Structures were solved by direct methods using the *SHELXS-97* package[13b] and refined with *SHELXL-97*.[13b] Calculations were performed using the *WinGX* system, version 1.80.03.[13c] The hydrogen atoms were located from the final difference Fourier map but were inserted at geometrically calculated positions and included in the refinement using the riding-model approximation; $U_{iso}$(H) was defined as 1.2$U_{eq}$ of the parent nitrogen atoms or the sp$^2$ carbon atoms and 1.5$U_{eq}$ of the parent carbon atoms for the methyl groups. There were disordered molecules present in the structure of **R-Zn$^{2+}$**. Because no obvious major site occupations were found for those molecules, it was not possible to model them. *PLATON/SQUEEZE*[13d] was used to correct the data, and a potential volume of 1342.0 Å$^3$ was found with 338 electrons per unit cell worth of scattering. These were removed from the model and not included in the empirical formula. The modified data set improved the $R_1$ value by ca. 56%. The electron count suggests the presence of two nitrate anions, thus accounting for charge balancing, and one molecule of methanol per unit cell. Least-squares refinements with anisotropic thermal motion parameters for all of the non-hydrogen atoms and isotropic ones for the remaining atoms were employed. Crystallographic data are summarized in Table S1 in the Supporting Information (SI), and selected bond distances and angles are presented in Table S2 in the SI.

**Anion-Sensing Studies.** Stock solutions ($1 \times 10^{-3}$ M) of the potassium salts of $F^-$, $Cl^-$, $Br^-$, $I^-$, $CH_3COO^-$, $CO_3^{2-}$, $HCO_3^-$, $N_3^-$, $SO_4^{2-}$, $PO_4^{3-}$, adenosine monophosphate (AMP), inorganic pyrophosphate (PPi), adenosine diphosphate (ADP), and adenosine trihosphate (ATP) were prepared in distilled water. A stock solution of the receptor **R-Zn$^{2+}$** ($1.0 \times 10^{-3}$ M) was also prepared: $CH_3CN$/*N*-2-hydroxyethylpiperazine-*N*′-2-ethanesulfonic acid (HEPES; 2:8, v/v; pH = 7.8). A 2 mL stock solution of **R-Zn$^{2+}$** was placed in a quartz cell of 1 cm width, and a tested cation solution was added in an incremental fashion. Corresponding fluorescence spectra were recorded at 298 K. Each titration was repeated at least two times to get a consistent value. For all measurements, $\lambda_{exc}$ = 360 nm and the emission wavelength was monitored at 400−700 nm. There was no considerable change in the shape of the emission spectra except a significant enhancement of the initial fluorescence intensity of **R-Zn$^{2+}$** upon the gradual addition of an anion solution. Analysis of the normalized fluorescence intensity ($I_0/I$) as a function of increasing guest concentration ([G]) was well described by the Stern−Volmer equation $I_0/I = 1 + K_{SV}[G]$. $K_{SV}$ was calculated from the slope of the Stern−Volmer plot.

**Cell Culture and Cytotoxicity Studies.** Human cervical (HeLa), breast cancer (MCF7), and breast epithelial (MCF10a) cell lines were obtained from the National Center for Cell Science, Pune, India, and the cancer cells (5 × 109/L) were plated on untreated glass coverslips coated with 0.2% gelatin for at least 1 h at room temperature and grown to 90% confluence in Dulbecco's modified eagle medium (DMEM) supplemented with 10% fetal calf serum (FCS), glutamine (2 mM), penicillin (100 units mL$^{-1}$), and streptomycin (100 $\mu$g mL$^{-1}$). The medium was removed and replaced with DMEM containing 1% serum prior to compound treatment. The base medium for this breast epithelial (MCF10a) cell line is DMEM/Ham's Nutrient Mixture F-12, catalog no. 51448C. To make the complete growth medium, add the following components to the base medium: horse serum, catalog no. H1270, to a final concentration (v/v) of 5%; cholera toxin, catalog no. C8052, to a final concentration of 1 ng mL$^{-1}$; human insulin, catalog no. I9278, to a final concentration of 10 $\mu$g mL$^{-1}$; epidermal growth factor, catalog no. E9644, to a final concentration of 10 ng mL$^{-1}$; hydrocortisone, catalog no. H6909, to a final concentration of 0.5 $\mu$g mL$^{-1}$. The cell viability was assessed by the MTT (3,4,5-dimethylthiazol-2-yl-2,5-diphenyltetrazolium bromide) method.


dx.doi.org/10.1021/ic500313m | *Inorg. Chem.* 2014, 53, 6655−6664

**Fluorescence Imaging.** The DMEM medium was removed from the cells and replaced with DMEM containing 1% serum prior to receptor **R** treatment. A $CH_3CN$/phosphate-buffered saline (PBS; 3:7, v/v) stock solution (1 mM) of **R** was diluted to 100 $\mu$M with DMEM and added to the cells in DMEM containing 1% FCS by bath application for a final dye concentration of 10 $\mu$M. The cells were incubated with the receptor **R** for 0.5 h at 37 °C and under 5% $CO_2$, washed with serum-free DMEM (2 × 2 mL), and bathed in serum-free DMEM (2 mL) before imaging. Experiments to assess the $Cu^{2+}$ and $Zn^{2+}$ uptake were performed in the same media supplemented with 10 $\mu$M $CuCl_2$ and $ZnCl_2$ for 1 h. Fluorescent images were captured on an ApoTome [Zeiss] fluorescence microscope and analyzed using the *Axio vision Rel 4.8* software.

**MTT Assay.** The cancer (HeLa and MCF7) and noncancer (MCF10a) cells were maintained in a humidified atmosphere containing 5% $CO_2$ at 37 °C in DMEM supplemented with 100 units of penicillin, 100 $\mu$g $mL^{-1}$ of streptomycin, and 10% fetal bovine serum. The capacity of the complex to interfere with the growth of HeLa, MCF7, and MCF10a cells was determined with the aid of MTT assay. Briefly, all of the cells with a density of $1 \times 10^4$ cells $well^{-1}$ were precultured in to 96-well microtiter plates for 48 h under 5% $CO_2$. The receptor **R**, $CuCl_2 \cdot 2H_2O$, $ZnCl_2 \cdot 6H_2O$, and complexes **R-Cu**$^{2+}$ and **R-Zn**$^{2+}$ were added in microwells containing the cell culture at concentrations of 2−100 $\mu$M. Then into each well was loaded 10 $\mu$L of a MTT solution (5 mg $mL^{-1}$ in PBS pH = 7.4) for 4 h at 37 °C. The insoluble formazan was dissolved in 100 $\mu$L of 4% DMSO, and the cell viability was determined by measuring the absorbance of each well at 570 nm using a Bio-Rad 680 microplate reader (Bio-Rad, USA). All experiments were performed in triplicate, and the percentage of cell viability was calculated according to the following equation. After 48 h, the cells were observed with an inverted phase contrast microscope and photographed with a Nikon FM 10 camera. Inhibition rate (IR %) = [OD(control) − OD(drug treated cell)]/[OD(control)] × 100%.

**Fluorescence Staining of HeLa Cells.** After 48 h, $IC_{50}$ concentrations of the $Cu^{2+}$, $Zn^{2+}$, receptor **R**, and complexes **R-Cu**$^{2+}$ and **R-Zn**$^{2+}$ were treated, and controlled cells were washed twice with 1X PBS buffer and stained with acridine orange/propidium iodide (AO/PI; 1:1, 10 $\mu$M) in a four-well Labtek II chambered cell for 15 min. Images were observed under the microscope. The appropriate amount of binding buffer added should be sufficient to ensure that the slide must not dry out during fluorescence microscopic observation. The cells were examined using a Plan-Neofluar 20× lens and then photographed as described above.

## RESULTS AND DISCUSSION

**Syntheses and Structural Analyses of Receptor R.** The present work stems from our interest in designing a new dual chemosensor **R** (Scheme 1) for $Cu^{2+}$ and $Zn^{2+}$ ions. It was

**Scheme 1. Synthesis of Chemosensor R**

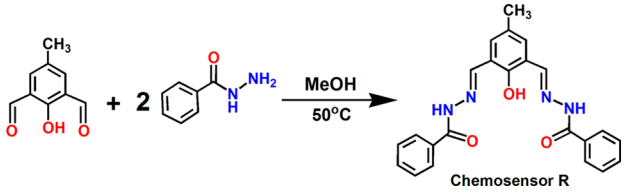


synthesized in a single step by reacting 2,6-diformyl-4-methylphenol with phenyl carbohydrazide in methanol (Scheme 1). The structure of **R** was fully characterized by FTIR, multinuclear ($^1H$ and $^{13}C$) NMR, ESI-MS, and elemental analyses. Its $^1H$ NMR in DMSO-$d^6$ (Figure S1 in the SI) indicates the high symmetry of the sensor, with only two sets of aromatic signals and a single resonance for the $CH_3$ and CH═N protons. The phenolic OH and NH protons appear at $\delta$ 12.34 and 12.15, respectively. In the $^{13}C$ NMR spectrum (Figure S2 in the SI), the signals of the C═N nuclei are observed at $\delta$ 163. The ESI-MS spectrum (Figure S3 in the SI) exhibits an intense peak at $m/z$ 423.23, which is assigned to [**R** + Na]$^+$. These spectroscopic and analytical data are consistent with the proposed formula of **R**.

The dimeric dicopper(II) **R-Cu**$^{2+}$ and dizinc(II) **R-Zn**$^{2+}$ complexes (Scheme 2) were synthesized by the addition of

**Scheme 2. Molecular Structure Representation of R-Cu$^{2+}$ and R-Zn$^{2+}$**

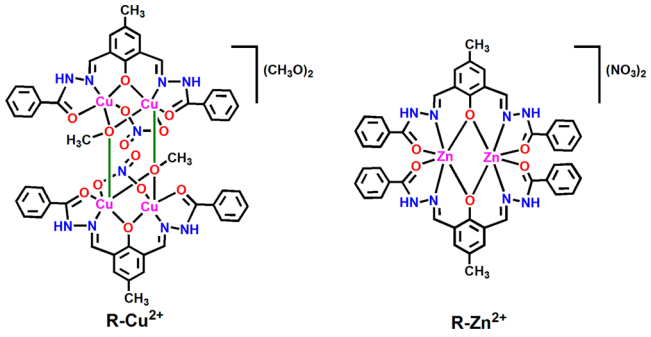


an ethanolic solution of copper(II) or zinc(II) chloride to a solution of the receptor **R** in ethanol. The crystal structures of **R-Cu**$^{2+}$ and **R-Zn**$^{2+}$ have been determined by single-crystal X-ray diffraction (XRD) analysis (see below). They reveal that the receptor **R** can bind with $Cu^{2+}$ and $Zn^{2+}$ ions in 1:2 and 1:1 ratios, respectively. The IR spectra clearly indicate the C═N stretching band of the chemosensor **R** at 1636 $cm^{-1}$. The presence of coordinated nitrate ions in **R-Cu**$^{2+}$ is indicated by the bands observed at around 1443 and 1246 $cm^{-1}$ because of the antisymmetric stretching and bending of nitrate ions, respectively. The difference between the aforesaid two frequencies (197 $cm^{-1}$) confirms the bidentate coordination of the nitrate ions.[14] The dizinc(II) complex **R-Zn**$^{2+}$ shows a strong band at 1359 $cm^{-1}$ and a sharp one at 822 $cm^{-1}$, which indicate the presence of uncoordinated nitrate ions in the crystal lattice. Both complexes (**R-Cu**$^{2+}$ and **R-Zn**$^{2+}$) are soluble in a $CH_3CN$/0.02 M HEPES (2:8, v/v) buffer at pH = 7.3 and exhibit three intense bands in the UV region (240−400 nm) attributed to the intraligand $\pi-\pi^*$ transitions within the coordinated phenolate moiety and imines. In the visible region, **R-Cu**$^{2+}$ exhibits an absorption maximum at 643 nm. This confirms[15] the square-based coordination geometry around copper(II) ions in **R-Cu**$^{2+}$.

Figure S4 in the SI shows the $^1H$ NMR spectral changes of **R** upon the addition of $Zn^{2+}$ in DMSO-$d^6$. After the addition of 1 equiv of $Zn^{2+}$ ions to **R**, the signal of the phenolic hydroxyl (OH) proton completely disappears and that of the NH proton decreases in intensity, confirming the 1:1 ratio between **R** and $Zn^{2+}$ in DMSO-$d^6$. The complex **R-Cu**$^{2+}$ (Figure S5 in the SI) shows ESI-MS peaks at $m/z$ 1079.62 and 557.15 corresponding to the $[Cu_4(R)_2(OCH_3) - 2NO_3 - 3OCH_3 + H^+]^+$ and $[Cu_2R(OCH_3) - OCH_3 - NO_3 + H^+]^+$ species, respectively. The complex **R-Zn**$^{2+}$ (Figure S6 in the SI) exhibits major peaks at $m/z$ 929.44 and 465.35, assigned to $[Zn_2(R)_2 - 2NO_3 + H^+]^+$ and $[Zn_2(R)_2 - 2NO_3]^{2+}$, respectively. These are consistent with the formulas observed in the single-crystal XRD and elemental analyses.

**Description of the Crystal Structure of R-Cu$^{2+}$.** The asymmetric unit of the copper(II) complex **R-Cu**$^{2+}$ (Figure 1)


dx.doi.org/10.1021/ic500313m | *Inorg. Chem.* 2014, 53, 6655−6664

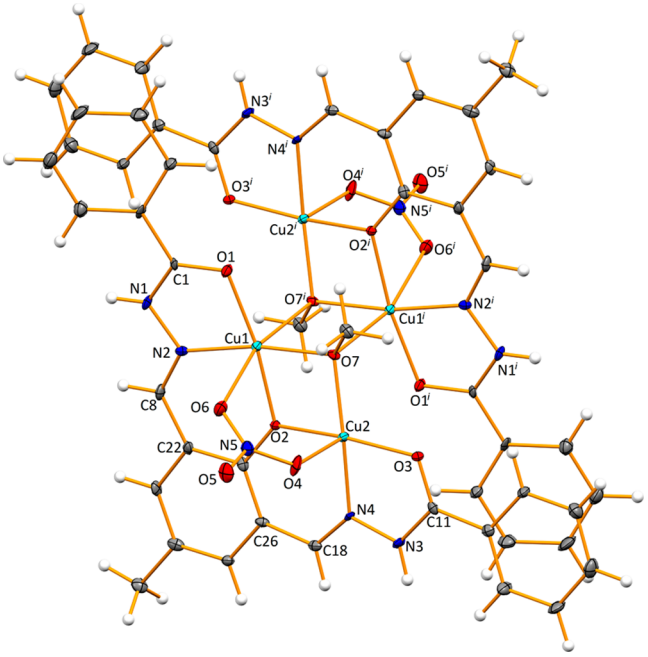


**Figure 1.** Crystal structure of the **R-Cu**$^{2+}$ complex. Ellipsoids are drawn at the 30% probability level. Symmetry operation to generate equivalent atoms: (i) $-x, -y, -z$. Methoxy anions are omitted for the sake of clarity.

contains half of the molecule, viz., a dinuclear entity made of two $Cu^{2+}$ cations with one R group, one methoxide, and one nitrate anion and a further methoxide anion as the counterion. The structure contains a crystallographically imposed inversion center in the middle of a $M_2(\mu_3\text{-}O)_2$ core, where M refers to Cu1 and the oxygen atoms (O7) belong to the methoxide ligands. By means of the O7 atoms, linkages are established to the Cu2 cations; the methoxide ligands, therefore, triply bridge three metals. Nitrate anions occur in syn−syn bridge-bonding modes. The R group acts as an $O_3N_2$ chelate, simultaneously binding Cu1 and Cu2, with the phenolate oxygen atom (O2) establishing a bridge between these cations. Consequently, another $M_2O_2$ unit can be found in the structure of **R-Cu**$^{2+}$, built with Cu2, Cu1, methoxide oxygen (O7), and phenolate oxygen (O2) atoms located in a plane that makes an angle of 80.68° with the previously indicated central dimetallic core (see above). Both the Cu1 and Cu2 cations exhibit distorted octahedral geometries (quadratic elongations of 1.063 and 1.070 and angle variances of 73.83 and 63.24°, respectively). However, for each metal cation, one of the metal−oxygen coordination distances [Cu1−O6 2.792(4) Å; Cu2−O1$^{i}$ 2.912(3) Å; Table S2 in the SI] considerably exceeds (by 0.4−0.6 Å) the others, but those dimensions are still within the sum of the van der Waals radii of the atoms involved. The shortest intrametallic distance found in this structure [2.9198(8) Å] relates the two copper atoms in the central $M_2O_2$ core and indicates a strong metal···metal interaction, comparable to those found in dicopper(II) sites of natural enzymes [e.g., catechol oxidase, $d$(Cu···Cu) = 2.90 Å][16] and shorter than those reported in exogenous alkoxo-bridged dicopper(II) complexes.[17] The structure is stabilized by means of intermolecular bond interactions involving the amide nitrogen atoms N1 and the O8 atoms from the methoxide counterions as acceptors [$d$(D···A) = 2.853(5) Å; ∠(D−H···A) = 154°]. Moreover, the structure features a 2D network by means of contact interactions involving the amide nitrogen atoms N3 and the O5 atoms from nitrate ligands of vicinal molecules [$d$(D···A) = 2.741(6) Å; ∠(D−H···A) 151°] (Figure S7 in the SI). Crystal data and details of data collection are reported in Table S1 in the SI, and selected bond lengths and angles are summarized in Table S2 in the SI.

**Description of the Crystal Structure of R-Zn$^{2+}$.** The asymmetric unit of the dinuclear zinc(II) complex **R-Zn**$^{2+}$ contains half of the molecule, with the metal cations occupying special positions and the binuclear $[Zn_2(R)_2]^{2+}$ unit being generated by means of a 2-fold axis passing through both metals (Figures 2 and S8 in the SI). The nitrate counterions are highly

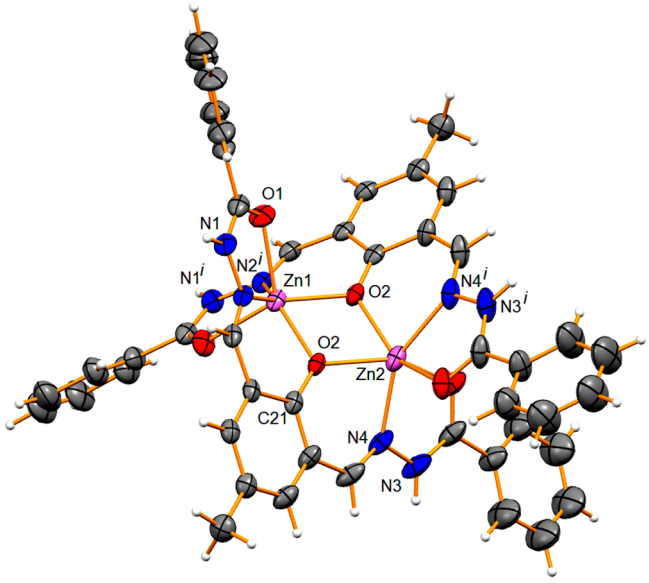


**Figure 2.** Crystal structure of the **R-Zn**$^{2+}$ complex. Ellipsoids are drawn at the 30% probability level. Symmetry operation to generate equivalent atoms: (i) $-x, y, 1.5 - z$.

disordered and believed to be located in voids (see the SI). In this compound, the receptor **R** also acts as a $O_3N_2$ chelator; both $Zn^{II}$ ions present highly distorted octahedral geometries, as expressed by the quadratic elongations of 1.157 and 1.115 and the angle variances of 451.64 and 357.52° for Zn1 and Zn2, respectively. Indeed, the major O−M−O or N−M−N angles found in the structure [144.65(13) or 150.6(2)°, respectively; Table S2 in the SI] are quite distant from the ideal 180°, giving, as a result, a considerable twisting of the **R** ligand and thus contrasting with what was found for **R-Cu**$^{2+}$. The zinc metal cations are bridged by the two phenoxide atoms (O2) of the receptor, thus forming a central $Zn_2O_2$ core, where the metals are 3.2757(9) Å apart.

**Sensing Studies.** The binding behavior of the chemosensor **R** toward different metal cations as their chloride salts was monitored using UV−visible absorption and fluorescence spectroscopy. All of the titration studies were carried out in a $CH_3CN$/0.02 M HEPES buffer at pH = 7.3. The electronic absorption spectrum of **R** (5 $\mu$M) exhibits two sharp bands at 300 and 363 nm (Figure 3). Upon the gradual addition of an aqueous solution of $Cu^{2+}$ and $Zn^{2+}$ ions in increasing concentration (0−10 $\mu$M), the bands at 345 and 332 nm, respectively, show significant increment in the absorption intensity. New absorption bands centered at 423 and 415 nm start to appear, being attributed to charge transfer in complexes **R-Cu**$^{2+}$ and **R-Zn**$^{2+}$, respectively (Figure 3). The appearance of


dx.doi.org/10.1021/ic500313m | Inorg. Chem. 2014, 53, 6655−6664

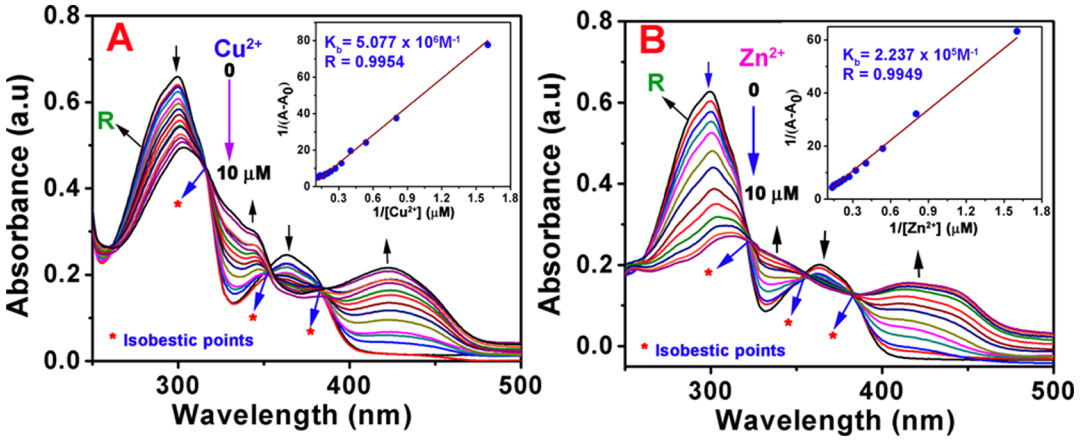


**Figure 3.** Change in the absorption spectrum of **R** (5 $\mu$M) in the presence of increasing concentration (0–10 $\mu$M) of $Cu^{2+}$ (A) and $Zn^{2+}$ (B) ions in a $CH_3CN$/0.02 M HEPES buffer (2:8, v/v) medium. Insets show the Benesi–Hildebrand plots.

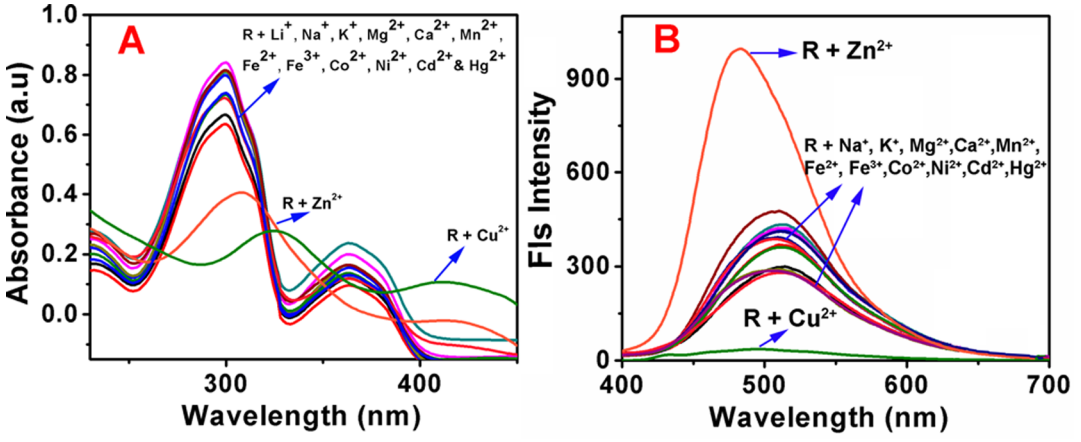


**Figure 4.** Change in the absorption spectrum (A) and initial fluorescence intensity (B) of chemosensor **R** (5 $\mu$M) upon mixing with different other metal cations in a $CH_3CN$/0.02 M HEPES buffer (2:8, v/v) medium.

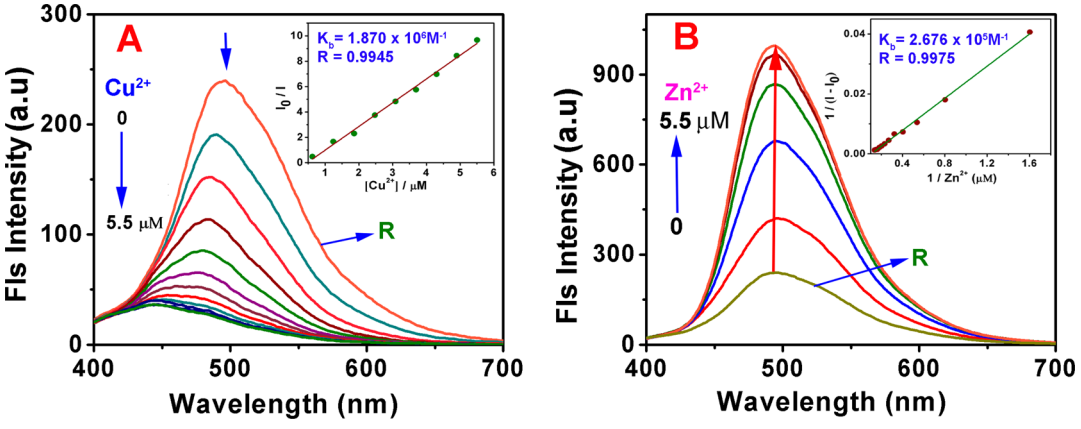


**Figure 5.** Change in the fluorescence spectra upon a gradual increase in the concentration of $Cu^{2+}$(A) and $Zn^{2+}$(B) (0–5.5 $\mu$M) in a $CH_3CN$/HEPES buffer (2:8, v/v) medium. Insets show the Stern–Volmer (A) and Benesi–Hildebrand (B) plots.

three well-defined isosbestic points centered at $\lambda$ = 316, 352, and 383 nm for **R**-$Cu^{2+}$ and $\lambda$ = 321, 355, and 384 nm for **R**-$Zn^{2+}$ is consistent with an equilibrium between **R** and **R**-$M^{2+}$ ($M^{2+}$ = $Cu^{2+}$ and $Zn^{2+}$) complexes, respectively, in solution.

Furthermore, perfect linear relationships were obtained from the absorption titration profiles for the plots measured $[1/(A - A_0)]$ at 423 nm (for **R**-$Cu^{2+}$) and 415 nm (for **R**-$Zn^{2+}$) as a function of $1/[M^{2+}]$ using the well-known linear Benesi–Hildebrand expression. The association constants of **R** with $Cu^{2+}$ and $Zn^{2+}$, $K_a$ = 5.08 × $10^6$ ($R$ = 0.9954) and 2.24 × $10^5$ $M^{-1}$ ($R$ = 0.9949), respectively, are obtained from the slope and intercept of these linear plots. Notably, the addition of other metal cations ($Na^+$, $K^+$, $Mg^{2+}$, $Ca^{2+}$, $Mn^{2+}$, $Fe^{2+}$, $Fe^{3+}$, $Co^{2+}$, $Ni^{2+}$, $Cd^{2+}$, and $Hg^{2+}$) did not alter the initial absorption spectrum of the chemosensor **R** significantly. From these absorption spectral studies, it is clear that the chemosensor **R**


dx.doi.org/10.1021/ic500313m | Inorg. Chem. 2014, 53, 6655–6664

shows a very high selective binding affinity in the ground state only for $Cu^{2+}$ and $Zn^{2+}$ ions even in the presence of other metal ions (Figure 4A).

The fluorescence spectrum of the chemosensor **R** (5 $\mu$M) exhibits a moderate emission at 493 nm in $CH_3CN$/0.02 M HEPES at pH = 7.3. Upon the gradual addition of increasing amounts of aqueous $Cu^{2+}$ solutions (0−5.5 $\mu$M) to the solution of **R**, the fluorescence emission at 493 nm is almost completely quenched after the addition of ∼2.0 equiv of $Cu^{2+}$ (Figure 5A). This dramatic quenching of the initial fluorescence intensity of **R** induced by $Cu^{2+}$ ion is attributed to the reverse photo-induced electron transfer (PET) from the 4-methylphenyl moiety to the phenolic OH and carbohydrazide nitrogen and oxygen atoms because of the decrease in the electron density upon $Cu^{2+}$ ion complexation.[18]

In contrast, the $Zn^{2+}$ ion caused the emission band to shift to a little longer wavelength at 497 nm, which significantly enhanced (∼4.1-fold increase) after the addition of ∼1.0 equiv of $Zn^{2+}$ (Figure 5B). The fluorescence enhancement of **R** in the presence of $Zn^{2+}$ may be due to the filled $d^{10}$ electronic configuration of the $Zn^{2+}$ ion, which does not usually involve any electron- or energy-transfer mechanisms for deactivation of the excited state.[19] The stoichiometry plot (Figure S9 in the SI) analysis of the fluorescence titration profile of **R** (5 $\mu$M) revealed a 1:2 and 1:1 stoichiometry between **R** and $Cu^{2+}$ and $Zn^{2+}$ species, respectively, and the corresponding calculated binding constants are $1.87 \times 10^6$ and $2.68 \times 10^5$ $M^{-1}$. The formation of 1:2 and 1:1 complexes was also indicated by XRD and ESI-MS, where the obtained spectra show peaks at $m/z$ 557.15 (**R-Cu$^{2+}$**) and 465.35 (**R-Zn$^{2+}$**) corresponding to the expected $[Cu_2R(OCH_3) - OCH_3 - NO_3 + H^+]^+$ and $[Zn_2(R)_2 - 2NO_3]^{2+}$ species, respectively.

In order to prove the selectivity of chemosensor **R** toward $Cu^{2+}$ and $Zn^{2+}$ ions, we carried out the fluorescence titration experiment of **R** with other alkali ($Na^+$ and $K^+$), alkali-earth ($Mg^{2+}$ and $Ca^{2+}$), and transition-metal ($Mn^{2+}$, $Fe^{2+}$, $Fe^{3+}$, $Co^{2+}$, $Ni^{2+}$, $Cd^{2+}$, and $Hg^{2+}$) ions. As shown in Figure 5B, only $Cu^{2+}$ and $Zn^{2+}$ elicited dramatic fluorescence quenching (9-fold) and enhancing (4-fold) responses, respectively, while the other tested metal ions exhibited almost no significant fluorescence quenching or enhancing responses (Figure S10 in the SI) under spectroscopic conditions identical with those used for $Cu^{2+}$ and $Zn^{2+}$.

To corroborate the high selectivity and sensitivity of **R** toward $Cu^{2+}$ over $Zn^{2+}$, the fluorescence intensity (Figure 5B) has been measured for chemosensors with both $Zn^{2+}$ and $Cu^{2+}$ ions. Surprisingly, the fluorescence intensity of **R** at 497 nm was dramatically quenched even in the presence of the diamagnetic component $Zn^{2+}$. Thus, chemosensor **R** could be used as a highly selective fluorescence sensor for the $Cu^{2+}$ ion over other metal species in an aqueous medium. The possible reason for the high selectivity of **R** might be due to the paramagnetic and incomplete d shell of the $Cu^{2+}$ ion. That eventually makes the $Cu^{2+}$ ion exhibit discernible quenching of the fluorescence intensity via electron- and/or energy-transfer process complex formation.[20]

To corroborate the practical applicability of chemosensor **R** as a selective fluorescence probe for $Cu^{2+}$ and $Zn^{2+}$ ions, we carried out a competitive fluorescence titration study with other competing metal ions. As shown in Figure S10 in the SI, the initial fluorescence intensity of **R** did not change significantly (green bar) upon mixing **R** with 1 equiv of different other metal cations ($Na^+$, $K^+$, $Mg^{2+}$, $Ca^{2+}$, $Mn^{2+}$, $Fe^{2+}$, $Fe^{3+}$, $Co^{2+}$, $Ni^{2+}$, $Cd^{2+}$, and $Hg^{2+}$). However, the subsequent addition of 1 equiv of $Cu^{2+}$ solution elicited a protuberant fluorescence quenching (red bar), which further confirmed the excellent selectivity of the sensor **R** for the $Cu^{2+}$ ion in an aqueous medium even in the presence of the other aforesaid potential interfering metal cations. Moreover, the search for visual sensors for trace detection of desired analytes has been a popular target in modern chemistry because of their ease of interpretation and use as a more suitable tool to practice in field. The ability of chemosensor **R** as a colorimetric probe for the $Cu^{2+}$ ion was imaged using a hand-held camera in the presence of other competing metal cations.

As depicted in Figure 6, **R** exhibits a distinct visual color change from colorless to yellowish green (under room light)

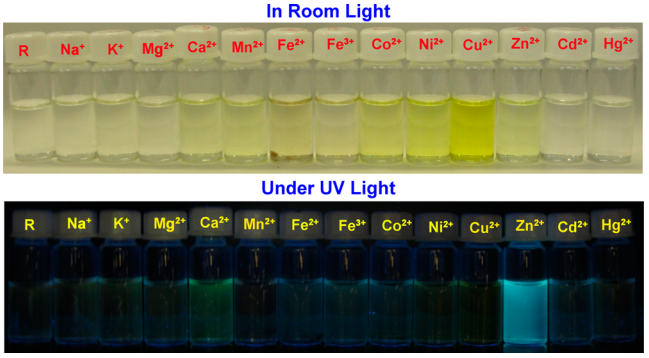


**Figure 6.** Visual color changes of chemosensor **R** (5.0 $\mu$M) upon the addition of 1 equiv of different metal ions in a $CH_3CN$/0.02 M HEPES buffer (2:8, v/v) medium.

and almost dark (under UV light) after the addition of a $Cu^{2+}$ solution. Under similar conditions, the chemosensor **R** displays almost dark-to-blue emission (under UV light) after the addition of a $Zn^{2+}$ solution. However, there was no observable color change noticed upon mixing of **R** with the aforesaid other potential interfering metal cation solutions. Thus, the chemosensor **R** can be used as a selective colorimetric sensor for $Cu^{2+}$ and $Zn^{2+}$ ions over other competing metal ions in various environmental and biological systems. As far as real-time application is concerned, the sensing process of a probe molecule must be a highly reversible one. To examine whether the sensing process of **R** is reversible, 1 equiv of a sodium salt of ethylendiaminetetraacetic acid (EDTA) solution was added into the solution of **R**, which was preincubated with 1 equiv of a $Cu^{2+}$/$Zn^{2+}$ solution. After the addition of an EDTA solution, the initial emission intensity of **R** was almost recovered immediately from nonfluorescent **R-Cu$^{2+}$** and fluorescent **R-Zn$^{2+}$** complexes (Figure S11 in the SI). This result suggests the high reversibility of **R** toward $Cu^{2+}$ and $Zn^{2+}$ sensing and the potential in application of real-time monitoring. In addition, the fluorescence titration profile also demonstrates that **R** has a detection limit of 0.272 nM (17.3 ppb) for $Cu^{2+}$ and 0.252 nM (16.5 ppb) for $Zn^{2+}$ ions (Figure S12 in the SI), which are comparable to the other reported $Cu^{2+}$ and $Zn^{2+}$ chemosensors,[11c,12,21,22] and this level of the detection limit is sufficient to sense $Cu^{2+}$ and $Zn^{2+}$ ions even in biological systems because the average concentration of $Cu^{2+}$ in blood is 100−150 $\mu$g $L^{-1}$ (15.7−23.6 $\mu$M).[23] Similarly, the total concentration of $Zn^{2+}$ ions in mammalian cells is estimated to be in the range of 100−500 $\mu$M;[24] the major fraction is


dx.doi.org/10.1021/ic500313m | Inorg. Chem. 2014, 53, 6655−6664

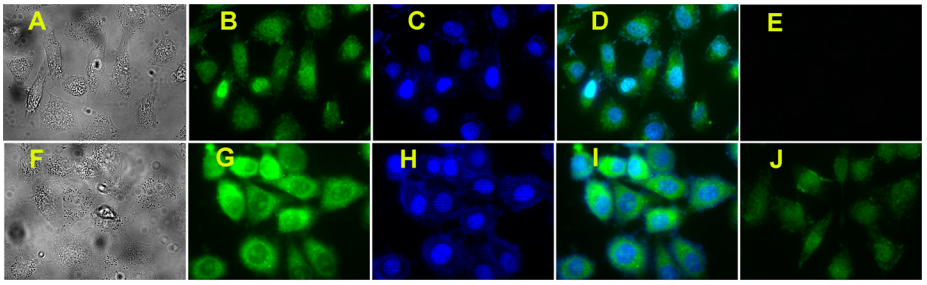


**Figure 7.** Fluorescence images of $Cu^{2+}$ and $Zn^{2+}$ in HeLa cells (ApoTome (Zeiss) confocal microscope; 40× objective lens). (A and F) Bright-field transmission images of HeLa cells. (B) Fluorescence images of HeLa cells supplemented with **R** (5 $\mu$M). (C and H) Hoechst 33342 stained image of HeLa cells incubated with **R** (5 $\mu$M) and **R** + $ZnCl_2$, respectively. (D) Merged images of B and C. (E and G) Cells incubated with **R** in the growth media for 0.5 h at 37 °C and then incubated with $CuCl_2$ (10 $\mu$M) and $ZnCl_2$ (10 $\mu$M), respectively, for 1 h at 37 °C. (I) Merged images of G and H. (J) Reversibility of fluorescence by adding EDTA (10 $\mu$M) to **R** + $CuCl_2$ treated HeLa cells.

**Table 1. Cytotoxicity ($IC_{50}$ Concentrations in $\mu$M) of R, R-$Cu^{2+}$, and R-$Zn^{2+}$ in Human Cancer and Noncancer Cell Lines**

| cell | R | R-$Cu^{2+}$ | R-$Zn^{2+}$ | $Cu^{2+}$ | $Zn^{2+}$ | cisplatin[26−28] |
|---|---|---|---|---|---|---|
| HeLa | 26.74 ± 2.3 | 04.15 ± 1.3 | 34.36 ± 3.4 | >100 | >100 | 3.80 |
| MCF7 | 22.52 ± 3.9 | 03.56 ± 2.4 | 31.00 ± 3.6 | >100 | >100 | 3.33 |
| MCF10a | 46.36 ± 3.8 | 38.42 ± 4.0 | 52.16 ± 4.3 | >100 | >100 | 91.00 ± 7.0 |

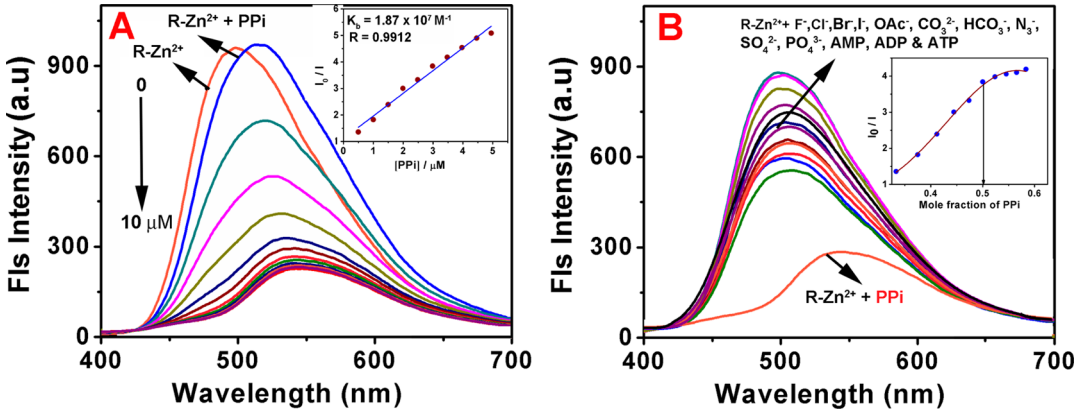


**Figure 8.** Changes in the initial fluorescence intensities of the receptor **R**-$Zn^{2+}$ (5 $\mu$M) in the presence of 1.0 equiv of different anions in 0.02 M HEPES at pH = 7.4 (left). Changes in the fluorescence spectra (right) upon the gradual increase in the concentration of PPi (0−50 $\mu$M). Insets show the Stern−Volmer (A) and Job's (B) plots.

tightly bound to metalloproteins, whereas a minor portion is bound to various readily exchangeable molecules.[25]

**Live Cell Imaging.** Having studied the interesting photophysical properties of **R**, such as high sensitivity, selectivity, and fast response toward $Cu^{2+}$ and $Zn^{2+}$ ions, we further extended our study to evaluate its potential use in imaging $Cu^{2+}$ and $Zn^{2+}$ ions in living cells. The human cervical HeLa cancer cell lines incubated for 0.5 h at 37 °C with **R** (5.0 $\mu$M) showed considerable fluorescence due to the accumulation of **R** within the cells (Figure 7). The addition of $Zn^{2+}$ (10.0 $\mu$M) to the preincubated cell for 1 h exhibited enhanced fluorescence intensity. However, in contrast, the staining of the preincubated cell with $Cu^{2+}$ (10.0 $\mu$M) for 1 h at 37 °C exhibited almost no fluorescence, and the subsequent addition of EDTA (10.0 $\mu$M) regenerated the initial emission intensity of **R**. This result implies that the chemosensor **R** is reversible and highly cell-membrane-permeable, and thus **R** can be used as a biosensor to probe the intracellular $Cu^{2+}$ and $Zn^{2+}$ concentrations and investigate their bioactivity in living cells.

**Cytotoxic Activity.** The antitumor potential of the receptor **R**, **R**-$Cu^{2+}$, and **R**-$Zn^{2+}$ toward human cervical cancer (HeLa) cells (Figure S13 in the SI) was evaluated by MTT assay. The cancer and noncancer cell lines were exposed to different concentrations of $Cu^{2+}$, $Zn^{2+}$, **R**, **R**-$Cu^{2+}$, and **R**-$Zn^{2+}$, and their $IC_{50}$ values were determined (Table 1). The antitumor activities follow the order $Zn^{2+}$ < $Cu^{2+}$ < **R**-$Zn^{2+}$ < **R** < **R**-$Cu^{2+}$. The complexes exhibit a considerable reduction in the viability of the cancer cells in a dose-dependent manner (Figure S13 in the SI). **R** and **R**-$Zn^{2+}$ have only a slight cytotoxicity ($IC_{50}$ > 35 $\mu$M) and could be used for intracellular detection (Table 1).

To evaluate the cell selectivity and anticancer potential, the $IC_{50}$ values of **R**-$Cu^{2+}$ and **R**-$Zn^{2+}$ toward two additional cell lines, MCF7 (breast cancer) and MCF10a (nonmalignant human breast epithelial cells), were determined. **R**-$Cu^{2+}$ shows ca. 4−5-fold selectivity toward breast and human cervical cancer cells (MCF7 and HeLa) over nonmalignant breast epithelial cells (MCF10a), demonstrating its potential as a novel anticancer agent (Table 1). **R**-$Cu^{2+}$ shows $IC_{50}$ values toward HeLa, MCF7, and MCF10a cells that are comparable to those of cisplatin[26−28] under identical conditions.

**Fluorescent Staining Method.** The characteristic morphological changes brought in the cells by treatment with $Cu^{2+}$, $Zn^{2+}$, **R**, **R**-$Cu^{2+}$, and **R**-$Zn^{2+}$ have been evaluated by


dx.doi.org/10.1021/ic500313m | Inorg. Chem. 2014, 53, 6655−6664

fluorescent microscopic analysis of AO/PI stained cells. The control viable cells have uniformly green fluorescing nuclei and a highly organized structure. After treating cells with $IC_{50}$ concentrations of those compounds for 48 h, we have observed cytological changes like late apoptotic cells that have orange-to-red fluorescing nuclei (Figure S14 in the SI) with condensed or fragmented chromatin; necrotic cells swollen to large sizes with uniformly orange-to-red fluorescing nuclei with no indication of chromatin fragmentation by staining. This indicates that the complexes **R**-$Cu^{2+}$ and **R**-$Zn^{2+}$ induce cell death through apoptosis, in contrast to **R** alone. **R**-$Cu^{2+}$ exhibits the strongest cytotoxic effect.

**Anion-Sensing Studies.** The binding behavior of the receptor **R**-$Zn^{2+}$ toward different anions was monitored using fluorescence and ESI-MS spectral techniques. All of the titration studies were carried out in a 0.02 M HEPES buffer at pH = 7.8. The fluorescence spectrum of the receptor **R**-$Zn^{2+}$ (5 $\mu$M) exhibits a strong emission at 497 nm in this medium. In the absence of any anions, **R**-$Zn^{2+}$ shows fluorescence at 497 nm upon excitation at 370 nm. This fluorescence emission is slightly changed upon the addition of an excess of $F^-$, $Cl^-$, $Br^-$, $I^-$, $CH_3COO^-$, $CO_3^{2-}$, $HCO_3^-$, $N_3^-$, $SO_4^{2-}$, Pi, AMP, ADP, and ATP. In contrast, the PPi anion caused the emission band to be shifted to a longer wavelength at 545 nm, which significantly quenched (~4.5-fold decrease) after the addition of ~1.0 equiv of PPi (Figure 8). This dramatic quenching of the initial fluorescence intensity of **R**-$Zn^{2+}$ is accounted for by the selective PET effect with PPi. Upon the addition of PPi, the emission is ca. 82% *switched off* or quenched because of the formation of the PPi–receptor complex. This is due to the anion recognition taking place through hydrogen bonding between charge-neutral recognition sites (here amide NH groups of the receptor **R**-$Zn^{2+}$) and PPi with concomitant changes in the photophysical properties of a fluorophore by modulation of a PET mechanism.[29,30] Such chemosensors should, in principle, show *ideal* PET behavior upon anion recognition.

By $^1$H NMR (Figure S15 in the SI), we have investigated the molecular interaction between **R**-$Zn^{2+}$ and PPi. Upon the addition of 1 equiv of PPi, the intensity of the NH proton signal ($\delta$ 12.09) decreases abruptly and disappears. At the same time, noticeable upfield chemical shifts are shown by all of the benzene ring protons (4-methylphenyl and benzoyl moieties) due to diamagnetic shielding of anionic species. This indicates a new complex formation between **R**-$Zn^{2+}$ and PPi by strong hydrogen-bonding interaction with the NH moiety and PPi, which results in deprotonation of the carbohydrazide NH group.[30] On the basis of the ESI-MS results, we assume that (at weak basic conditions) the dinuclear complex **R**-$Zn^{2+}$ decomposes into two discrete mononuclear ZnR($NO_3$) species, which interact with PPi through hydrogen bonding. The stoichiometry plot (Figure 8) analysis of the fluorescence titration profile of **R**-$Zn^{2+}$ (5 $\mu$M) also reveals a 1:1 stoichiometry between **R**-$Zn^{2+}$ and PPi species, and the calculated association constant is $1.87 \times 10^6$ $M^{-1}$ ($R$ = 0.991) [Figure 8A,B (insets)]. The formation of a 1:1 complex was further supported by ESI-MS data (Figure S16 in the SI), which detect a species at $m/z$ 174.88 corresponding to $[C_{23}H_{19}N_5O_{13}P_2Zn]^{4-}$ (=$[ZnR + PPi - 4K^+]^{4-}$).

In order to prove the selectivity of the receptor **R**-$Zn^{2+}$ toward PPi, we carried out the fluorescence titration experiments of **R**-$Zn^{2+}$ with other aforesaid anions. As shown in Figure 8B, only PPi elicited a significant fluorescence quenching response, while the other tested anions exhibited almost similar fluorescence responses under spectroscopic conditions identical with those applied for PPi. Thus, the receptor **R**-$Zn^{2+}$ could be used as a highly selective fluorescence sensor for PPi over other anionic species in an aqueous medium. To corroborate the practical applicability of **R**-$Zn^{2+}$ as a selective fluorescence probe for PPi, we carried out a competitive fluorescence titration study with other competing anions. As shown in Figure S17 in the SI, the initial fluorescence intensity of **R**-$Zn^{2+}$ changed considerably (green bars) upon mixing with 1 equiv of any of the other above-mentioned anions. However, the subsequent addition of 1 equiv of a PPi solution caused a prominent fluorescence quenching (red bars), which further confirmed the excellent selectivity of the sensor **R**-$Zn^{2+}$ for PPi in an aqueous medium even in the presence of such potential interfering anions.

Although related phosphate analogues, such as $PO_4^{3-}$, AMP, ADP, and ATP, considerably decreased the fluorescence intensity, their binding propensity with **R**-$Zn^{2+}$ was not sufficiently strong to enable the PET mechanism. Moreover, the search for visual sensors for trace detection of desired analytes has been a popular target because of their ease of interpretation and use as a more suitable tool in the field. The ability of the receptor **R**-$Zn^{2+}$ as a colorimetric probe for PPi was imaged using a hand-held camera in the presence of other competing anions. As depicted in Figure S18 in the SI, **R**-$Zn^{2+}$ exhibits a distinct visual color change from blue emission to almost colorless (under UV light) after the addition of a PPi solution. However, there are no considerable color changes upon mixing **R**-$Zn^{2+}$ with any of the other aforesaid anion solutions. Thus, **R**-$Zn^{2+}$ can be used as a selective colorimetric sensor for PPi over other competing anions in various environmental and biological systems. In addition, the fluorescence titration profiles also demonstrate that the receptor **R**-$Zn^{2+}$ has a detection limit (Figure S19 in the SI) of $7.16 \times 10^{-9}$ M (123 ppb) for PPi, which is comparable to those for reported PPi chemosensors.[2a,31]

## CONCLUSIONS

We have designed a new benzoyl hydrazone based chemosensor **R**, which shows highly selective, sensitive, and reversible fluorescence *off–on* responses toward $Cu^{2+}$ and $Zn^{2+}$ in an aqueous medium. On the basis of the sensing studies, **R** displays efficient sensitivity and selectivity toward $Cu^{2+}$ rather than $Zn^{2+}$ ions. In addition, we further demonstrated that this new chemosensor can be utilized in live cell imaging of $Cu^{2+}$ and $Zn^{2+}$ ions. The excellent detection limits of 17.3 and 16.5 ppb of this chemosensor **R** toward $Cu^{2+}$ and $Zn^{2+}$ ions, respectively, can be useful in the detection of trace quantities of $Cu^{2+}$ and $Zn^{2+}$ ions in biological and environmental samples. Also, in terms of the expected membrane permeability and nontoxic nature, **R** can be a very important sensing probe for the detection of $Cu^{2+}$ and $Zn^{2+}$ in living cells.

Biochemical studies on the cytotoxicity reveal that the copper(II) and zinc(II) complexes of the receptor, **R**-$Cu^{2+}$ and **R**-$Zn^{2+}$, act as anticancer agents by inducing phenotypical changes and increasing the membrane permeability, which is consistent with the induction of mainly apoptotic cell death. Further mechanistic and cellular uptake studies are essential to probing the higher potency of these complexes to kill cancer cells, and efforts are in progress for a similar kind of fluorogenic probe. In addition, the dizinc(II) complex **R**-$Zn^{2+}$ shows a selective and sensitive fluorescence response (detection limit =


dx.doi.org/10.1021/ic500313m | Inorg. Chem. 2014, 53, 6655–6664

123 ppb) toward PPi over the structurally similar phosphates Pi, AMP, ADP, and ATP and other anions in an aqueous medium.

Interestingly, the dimeric dicopper(II) complex (**R-Cu$^{2+}$**) can act as a catalyst in catechol and alcohol oxidation reactions, a study that is reported separately.

## ■ ASSOCIATED CONTENT

### Supporting Information

X-ray crystallographic file in CIF format and data of sensor, bioimaging, and cytotoxicity studies for the compounds. This material is available free of charge via the Internet at http://pubs.acs.org.

## ■ AUTHOR INFORMATION


### Corresponding Author

*E-mail: pombeiro@tecnico.ulisboa.pt.


### Author Contributions

This manuscript was written through contributions of all authors and approved to the final version of the manuscript. These authors contributed equally.

### Notes

The authors declare no competing financial interest.

## ■ ACKNOWLEDGMENTS

S.A. is grateful to the Foundation for Science and Technology (FCT), Portugal, for the award of a postdoctoral fellowship (ref: SFRH/BPD/76451/2011). This work has also been partially supported by the FCT Project Pest-OE/QUI/UI0100/2013. R.R. is thankful to the CSIR, New Delhi, India, for a senior research fellowship.

## ■ REFERENCES


(1) Que, E. L.; Domailli, D. W.; Chang, C. J. *Chem. Rev.* **2008**, *108*, 1517.

(2) (a) Manez, R. M.; Sancenon, F. *Chem. Rev.* **2003**, *103*, 4419. (b) Kim, J. S.; Quang, D. T. *Chem. Rev.* **2007**, *107*, 3780.

(3) Da silva, J. J. R. F.; Williams, R. J. P. *The Biological Chemistry of the Elements*; Clarendon Press: Gloucestershire, U.K., 1991.

(4) Halliwell, B.; Gutteridge, J. M. *Biochem. J.* **1984**, *219*, 1.

(5) (a) Sarkar, B. *Chem. Rev.* **1999**, *99*, 2535. (b) Barnham, K. J.; Masters, C. L.; Bush, A. I. *Nat. Rev. Drug Discovery* **2004**, *3*, 205.

(6) Emami, S.; Hosseinimehr, S. J.; Taghdisi, S. M.; Akhlaghpoor, S. *Bioorg. Med. Chem. Lett.* **2007**, *17*, 45.

(7) Huang, Q.; Pan, Z.; Wang, P.; Chen, Z.; Zhang, X.; Xu, H. *Bioorg. Med. Chem. Lett.* **2006**, *16*, 3030.

(8) (a) Nakayama, A.; Hiromura, M.; Adachi, Y.; Sakurai, H. *J. Biol. Inorg. Chem.* **2008**, *13*, 675. (b) Sakurai, H.; Yoshikawa, Y.; Yasui, H. *Chem. Soc. Rev.* **2008**, *7*, 2383.

(9) (a) Chohan, Z. H.; Arif, M.; Sarfraz, M. *Appl. Organomet. Chem.* **2007**, *21*, 294. (b) Singh, V. P.; Katiyar, A. *J. Coord. Chem.* **2008**, *61*, 3200. (c) Kaczmarek, M. T.; Jastrza, R.; Hołderna-Kedzia, E.; Radecka-Paryzek, W. *Inorg. Chim. Acta* **2009**, *362*, 3127. (d) Anbu, S.; Kamalraj, S.; Varghese, B.; Muthumary, J.; Kandaswamy, M. *Inorg. Chem.* **2012**, *51*, 5580.

(10) Ali, M. M.; Frei, E.; Straubb, J.; Breuerb, A.; Wiesslerb, M. *Toxicology* **2002**, *85*, 179.

(11) (a) Wang, J.; Lin, W.; Yuan, L.; Song, J.; Gao, W. *Chem. Commun.* **2011**, *47*, 12506. (b) Huang, L.; Cheng, J.; Xie, K.; Xi, P.; Hou, F.; Li, Z.; Xie, G.; Shi, Y.; Liu, H.; Bai, D.; Zeng, Z. *Dalton Trans.* **2011**, *40*, 10815. (c) Simmons, J. T.; Allen, J. R.; Morris, D. R.; Clark, R. J.; Levenson, C. W.; Davidson, M. W.; Zhu, L. *Inorg. Chem.* **2013**, *52*, 5338. (d) Nowakowski, A. B.; Petering, D. H. *Inorg. Chem.* **2011**, *50*, 10124.

(12) (a) Ahamed, B. N.; Ravikumar, I.; Ghosh, P. *New J. Chem.* **2009**, *33*, 1825. (b) Tan, Y.; Gao, J.; Yu, J.; Wang, Z.; Cui, Y.; Yang, Y.; Qian, G. *Dalton Trans.* **2013**, *42*, 11465.

(13) (a) *APEX2* and *SAINT*; Bruker AXS Inc.: Madison, WI, 2004. (b) Sheldrick, G. M. *Acta Crystallogr., Sect. A: Found. Crystallogr.* **2008**, *64*, 112. (c) Farrugia, L. J. *J. Appl. Crystallogr.* **1999**, *32*, 837. (d) Spek, A. L. *Acta Crystallogr., Sect. A: Found. Crystallogr.* **1990**, *46*, C34.

(14) Gatehouse, B. M.; Livingstone, S. E.; Nyholm, R. S. *J. Inorg. Nucl. Chem.* **1958**, *8*, 75.

(15) Okawa, H.; Tadocara, M.; Aratake, T. K.; Ohba, M.; Shindom, K.; Mitsumi, M.; Koikawa, M.; Tomono, M.; Fenton, D. E. *J. Chem. Soc., Dalton Trans.* **1993**, 253.

(16) Klabunde, T.; Eicken, C.; Sacchettini, J. C.; Krebs, B. *Nat. Struct. Biol.* **1998**, *5*, 1084.

(17) (a) Fernandes, C.; Neves, A.; Bortoluzzi, A. J.; Mangrich, A. S.; Rentschler, E.; Szpoganicz, B.; Schwingel, E. *Inorg. Chim. Acta* **2001**, *320*, 12. (b) Murthy, N. N.; Karlin, K. D.; Berini, C.; Luchinat, J. *J. Am. Chem. Soc.* **1997**, *119*, 2156. (c) Drew, M. G. B.; Yates, P. C.; Esho, F. S.; Grimshaw, J. T.; Lavery, A.; McKillop, K. P.; Nelson, S. M.; Nelson, J. *J. Chem. Soc., Dalton Trans.* **1988**, 2995. (d) Landers, A. E.; Philips, D. J. *Inorg. Chim. Acta* **1979**, *32*, 53.

(18) Kumar, M.; Kumar, R.; Bhalla, V.; Sharma, P. R.; Kaur, T.; Qurishi, Y. *Dalton Trans.* **2012**, *41*, 408.

(19) (a) Czarnik, A. W. *Fluorescent Chemosensors for Ion and Molecule Recognition*; American Chemical Society: Washington, DC, 1992. (b) Sinkeldam, R. W.; Greco, N. J.; Tor, Y. *Chem. Rev.* **2010**, *110*, 2579.

(20) (a) Jung, H. S.; Kwon, P. S.; Lee, J. W.; Kim, J. I.; Hong, C. S.; Kim, J. W.; Yan, S.; Lee, J. Y.; Lee, J. H.; Joo, T.; Kim, J. S. *J. Am. Chem. Soc.* **2009**, *131*, 2008. (b) Li, Z.; Zhang, L.; Wang, L.; Guo, Y.; Cai, L.; Yu, M.; Wei, L. *Chem. Commun.* **2011**, *47*, 5798.

(21) (a) Qin, H.; Ren, J.; Wang, J.; Wang, E. *Chem. Commun.* **2010**, *46*, 7385. (b) Zhao, X. Y.; Liu, Y.; Schanze, K. S. *Chem. Commun.* **2007**, 2914. (c) Beltramello, M.; Gatos, M.; Mancin, F.; Tecillab, P.; Tonellatoa, U. *Tetrahedron Lett.* **2001**, *42*, 9143. (d) Huang, L.; Chen, F.; Xi, P.; Xie, G.; Li, Z.; Shi, Y.; Xu, M.; Liu, H.; Maa, Z.; Bai, D.; Zeng, Z. *Dyes Pigm.* **2011**, *90*, 265.

(22) (a) Midya, G. C.; Paladhi, S.; Bhowmik, S.; Sahaa, S.; Dash, J. *Org. Biomol. Chem.* **2013**, *11*, 3057. (b) Simmons, J. T.; Allen, J. R.; Morris, D. R.; Clark, R. J.; Levenson, C. W.; Davidson, M. W.; Zhu, L. *Inorg. Chem.* **2013**, *52*, 5838.

(23) Tak, W. T.; Yoon, S. C. *Korean. J. Nephrol.* **2001**, *20*, 863.

(24) Eide, D. J. *Biochim. Biophys. Acta* **2006**, *1763*, 711.

(25) (a) Maret, W.; Krezel, A. *Mol. Med.* **2007**, *13*, 371. (b) Lin, W.; Buccella, D.; Lippard, S. J. *J. Am. Chem. Soc.* **2013**, *135*, 13512.

(26) Tak, W. T.; Yoon, S. C. *Korean J. Nephrol.* **2001**, *20*, 863.

(27) Eide, D. J. *Biochim. Biophys. Acta* **2006**, *1763*, 711.

(28) (a) Maret, W.; Krezel, A. *Mol. Med.* **2007**, *13*, 371. (b) Lin, W.; Buccella, D.; Lippard, S. J. *J. Am. Chem. Soc.* **2013**, *135*, 13512.

(29) (a) Gunnlaugsson, T.; Davis, A. P.; O'Brien, J. E.; Glynn, M. *Org. Lett.* **2002**, *4*, 2449. (b) Pathak, R. K.; Hinge, V. K.; Rai, A.; Panda, D.; Rao, C. P. *Inorg. Chem.* **2011**, *17*, 13999. (c) Rurack, K. *Spectrochim. Acta, Part A* **2001**, *57*, 2161. (d) Amendola, V.; Fabbrizzi, L.; Mangano, C.; Pallavicini, P. *Acc. Chem. Res.* **2001**, *34*, 488. (e) deSilva, A. P.; Gunaratne, H. Q. N.; Gunnlaugsson, T.; Huxley, A. J. M.; McCoy, C. P.; Rademacher, J. T.; Rice, T. E. *Chem. Rev.* **1997**, *97*, 1515.

(30) (a) Linton, B. R.; Goodman, M. S.; Fan, E.; van Arman, S. A.; Hamilton, A. D. *J. Org. Chem.* **2001**, *66*, 7313. (b) Buhlmann, P.; Nishizawa, S.; Xiao, K. P.; Umezawa, Y. *Tetrahedron* **1997**, *53*, 1647. (c) Kelly, R. R.; Kim, M. H. *J. Am. Chem. Soc.* **1994**, *116*, 7072. (d) Fan, E.; van Arman, S. A.; Kincaid, S.; Hamilton, A. D. *J. Am. Chem. Soc.* **1993**, *115*, 369. (e) Dixon, R. P.; Geib, S. J.; Hamilton, A. D. *J. Am. Chem. Soc.* **1992**, *114*, 365. (f) Garcia-Tellado, F.; Goswami, S.; Chang, S.-K.; Geib, S. J.; Hamilton, A. D. *J. Am. Chem. Soc.* **1990**, *112*, 7393. (g) Peng, X.; Wu, Y.; Fan, J.; Tian, M.; Han, K. *J. Org. Chem.* **2005**, *70*, 10524.

(31) (a) Martınez-Manez, R.; Sancanon, F. *Chem. Rev.* **2003**, *103*, 4419. (b) Liao, J.-H.; Chen, C.-T.; Fang, J.-M. *Org. Lett.* **2002**, *4*, 561.

(c) Anbu, S.; Kamalraj, S.; Jayabaskaran, C.; Mukherjee, P. S. *Inorg. Chem.* **2013**, *52*, 8294.